scientific reports

Check for updates

OPEN

Mapping partial agonism of mitragynine at the μ-opioid receptor through molecular dynamics and Markov state modelling analysis

Mohammad Nazri Abdul Bahari[1], Liyana Azmi[2], Low Chen Fei[3], Amir Syahir[4], Enoch Perimal[5], Asrulnizam Abd Manaf[1] & Muhamad Arif Mohamad Jamali[6]✉

Mitragynine, a major indole alkaloid from *Mitragyna speciosa* (kratom), acts as a partial agonist at the μ-opioid receptor (μOR), yet the structural basis for its submaximal efficacy remains unclear. Here, we integrate microsecond-scale all-atom molecular dynamics (MD) simulations with Markov State Modelling (MSM) to probe how mitragynine modulates μOR conformational landscapes and kinetics versus a morphine-bound control. MD in explicit POPC bilayers quantified backbone stability, residue-level flexibility, global compactness, and hydrogen bonding. MMPBSA calculations indicated favourable binding for both ligands, with a more negative ΔG_bind for mitragynine (–16.3 ± 5.1 kcal mol⁻¹) than morphine (–10.8 ± 4.2 kcal mol⁻¹). MSMs built on TM3–TM6 separations, DRY/NPxxY χ_1 torsions, and ICL distances revealed distinct energy landscapes: morphine stabilised a deep active-like basin, whereas mitragynine broadened sampling of intermediate basins and reduced occupancy of fully active conformations. Kinetic analysis showed shorter intermediate→open transition times for morphine (hundreds of nanoseconds) but markedly longer, microsecond-scale transitions for mitragynine, yielding macrostate populations enriched in intermediates for mitragynine and in closed/open states for morphine. Together, these data provide a mechanistic explanation for mitragynine's partial, G-protein-biased agonism at μOR and a quantitative framework to guide the design of biased μOR ligands.

Keywords Mitragynine, μ-opioid receptor, Markov state modelling analysis, Molecular dynamics simulation, Partial agonist

G-protein-coupled receptors (GPCRs) comprised of a large superfamily of membrane proteins that mediate diverse physiological processes[1]. The μ-opioid receptor (μOR) is a class A GPCR that mediate pain perception and analgesia. Strong analgesic effects are produced through intracellular G-protein signalling upon agonist binding to μOR. However, classical full-agonist opioids, for instance, the morphine and fentanyl exhibit high efficacy in pain suppression, their clinical utility is hindered by severe side effects such as respiratory depression, tolerance, and high abuse liability that is correlated to β-arrestin-dependent signalling[1–3]. These drawbacks have driven the exploration of novel opioid ligands with improved safety profiles. For example, analgesia with reduced side effects that can be achieved by partial agonists; or arrestin-mediated pathways that can be minimized by G-protein-biased agonists[4,5]. Mitragynine, a naturally occurring indole alkaloid extracted from the Southeast

[1]Collaborative Microelectronic Design Excellence Center (CEDEC), Universiti Sains Malaysia, No. 10, Persiaran Bukit Jambul, 11900 Bayan Lepas, Pulau Pinang, Malaysia. [2]Faculty of Medicine and Health Sciences, Universiti Sains Islam Malaysia, 71800 Nilai, Negeri Sembilan, Malaysia. [3]Institute of Systems Biology, Universiti Kebangsaan Malaysia (UKM), 43600 Bangi, Selangor, Malaysia. [4]Nanobiotechnology Research Group, Department of Biochemistry, Faculty of Biotechnology and Biomolecular Sciences, Universiti Putra Malaysia (UPM), 43400 Serdang, Selangor, Malaysia. [5]Curtin Medical School, Faculty of Health Sciences, Curtin University, Kent St, Bentley, WA 6102, Australia. [6]Faculty of Science and Technology, Universiti Sains Islam Malaysia, 71800 Nilai, Negeri Sembilan, Malaysia. ✉email: arifjamali@usim.edu.my

Asian plant *Mitragyna speciosa* (kratom), has emerged as a promising candidate in this regard. Studies have shown that mitragynine produces opioid-like analgesia with minimal adverse effect. It has been reported to bind not only to the μ-opioid receptor, but also to the δ- and κ-opioid receptors with nanomolar affinity. Mitragynine has been reported to activate G-protein signalling at μOR without detectable β-arrestin-2 recruitment[5,6] and these features have led to the hypothesis that mitragynine may produce analgesia while avoiding classical opioid liabilities[4,6]. Supporting behavioural studies showed that mitragynine can ameliorate opioid withdrawal symptoms and produce opioid-like effects in humans and rodents with milder safety profiles[6,7]. While its pharmacological profile has been described in vitro and in vivo, the structural and dynamic mechanisms underlying mitragynine's partial efficacy remain unclear.

Recent crystallographic and computational work has highlighted key conserved motifs in GPCR activation, included DRY motif in transmembrane helix 3, the NPxxY motif in transmembrane helix 7, and the tryptophan toggle-switch W^6.48 in transmembrane helix 6 that undergo characteristic rearrangements upon activation[8,9]. A partial agonist was hypothesized to induce only a subset of conformational changes among these motifs that lead to attenuated signalling. In this context, computational approaches are well suited to capture the dynamic conformational differences in GPCRs activation induced by full and partial agonists[10]. Molecular dynamics simulation is one of the computational approaches that precisely predict atomistic trajectories of protein dynamics, revealing residues fluctuation and reorientation in response to different ligands[11–14]. Nonetheless, GPCR activation involves rare events on long timescales that requires extensive sampling to adequately capture the full spectrum of conformational transitions and intermediate states associated with ligand efficacy[15–18]. To address this, advanced ensemble-sampling techniques were used to construct Markov state models (MSMs) from short and long trajectories to effectively map out the kinetic landscape of receptor protein conformations[10,19,20]. Recent molecular dynamics studies combined with MSMs have mapped the energy landscapes of activation for many GPCRs, uncovered multiple activation pathways and metastable states that depend on ligand efficacy. For instance, MSM analyses revealed that partial agonists such as Δ^9- tetrahydrocannabinol (THC) in cannabinoid receptor (CB1R)[21,22] or glucagon alone in glucagon receptor (GCGR)[23] induced intermediate or less stable active conformations, compared to full agonists and G proteins, which stabilized well-defined active basins. In this context, partial agonists appeared to bias receptors toward intermediate states that weakly activated G proteins, while full agonists induced the ensemble into deep active basins. However, despite the growing application of MSMs in GPCR studies, the dynamic ensemble-based analyses remain underexplored for μ-opioid receptor.

In this study, 1 μs all-atom MD simulations of mitragynine-bound and morphine-bound μ-opioid receptor were conducted in a lipid bilayer environment to dissect the conformational landscapes, structural dynamics, and kinetic transitions induced by different ligands. A combination of MMPBSA binding free energy calculations, tICA, and MSM-based kinetic modelling was applied to evaluate the behaviour of the receptor in response to specific ligand binding. This computational framework aimed to elucidate the activation and stability of μ-opioid receptor conformations upon mitragynine binding that contribute to its partial and biased agonism. Findings from the current analyses not only aligned with prior experimental data but also provided mechanistic insights that may guide the rational design of next-generation opioids with improved safety profiles.

Methodology

Ligand preparation and molecular docking

The structure of mitragynine (PubChem CID: 107887) was retrieved from the PubChem database and geometry-optimized using the MMFF94 force field in Avogadro 1.2.0. The active-state structure of the μ-opioid receptor (μOR) in complex with morphine (PDB ID: 8EF6)[24] was used as the control, representing a high-resolution conformation of the receptor. Structural preprocessing was performed in UCSF Chimera, where water molecules and heteroatoms were removed, hydrogen atoms were added, and Gasteiger charges were assigned. Flexible ligand docking was conducted using AutoDock Vina (v1.2.3), with the grid box centered on the orthosteric binding pocket based on morphine's coordinates (grid dimensions: 24 × 24 × 24 Å). The top-ranked binding pose of mitragynine was selected for downstream modeling, ensuring proper alignment with key μOR residues, including Asp147^3.32, Tyr148^3.33, and His297^6.52.

System setup with CHARMM-GUI membrane builder

The protein–ligand complexes (μOR-morphine and μOR-mitragynine) were subjected to the CHARMM-GUI Membrane Builder (June 2024 release) for system preparation. Each complex was embedded within a symmetric lipid bilayer composed of 220 POPC lipids. The systems were solvated using TIP3P water, with a 20 Å buffer above and below the membrane. Counterions and 0.15 M KCl were added to achieve electroneutrality and physiological ionic strength. Force field parameters were assigned using CHARMM36m for the protein, lipids, and ligands. Mitragynine ligand topology was generated via CGenFF server and manually curated to ensure compatibility with CHARMM36m standards.

Molecular dynamics simulations

Molecular dynamics (MD) simulations were performed using GROMACS 2024.2 with CUDA acceleration on RTX 4090-based workstations. The default CHARMM-GUI six-step equilibration protocol was executed, comprising two NVT phases (125 ps total) with restrained heavy atoms and four NPT phases (1.5 ns total) with gradually reduced restraints. Production simulations were run for 1000 ns in the NPT ensemble with a 2 fs time step. Temperature was maintained at 310 K using the Nosé–Hoover thermostat, while pressure was controlled semi-isotropically at 1 bar using the Parrinello–Rahman barostat ($\tau = 5$ ps). Long-range electrostatics were treated using the Particle Mesh Ewald (PME) method with a cutoff of 1.2 nm. All covalent bonds involving hydrogen atoms were constrained using LINCS algorithm. Trajectory frames were saved every 10 ps. Post-processing of simulation trajectories was performed using gmx trjconv to remove periodic boundary conditions

and re-center the protein within the simulation box. Three independent 1 μs MD simulations were performed for each ligand using distinct random seeds to ensure reproducibility.

Trajectory-based structural analysis

Root mean square deviation (RMSD), root mean square fluctuation (RMSF), and radius of gyration (Rg) analyses were conducted using gmx rms, gmx rmsf, and gmx gyrate, respectively, over the full 1000 ns production trajectory. Structural deviations were referenced against the initial energy-minimized structures. Per-residue flexibility profiles were generated to compare the morphine- and mitragynine-bound μOR complexes, with particular focus on transmembrane helices and key microswitch motifs, including NPxxY, DRY, and the toggle switch residue W^6.48. Hydrogen bonding patterns were assessed using gmx hbond. For each ligand, the three 1 μs trajectories were concatenated and used to compute a single covariance matrix for PCA (GROMACS gmx covar). The resulting eigenvectors were then used to project each replicate individually (gmx anaeig), enabling direct comparison of replicate sampling in the same PC space.

MMPBSA binding energy calculation

Binding free energy was computed using gmx_MMPBSA v1.5.3, adopting a single-trajectory approach over the final 100 ns of each simulation. Trajectory frames were extracted every 20 ps intervals, yielding 5000 frames per protein-ligand complex. The binding energy (ΔG_bind) components included van der Waals interactions, electrostatics, polar solvation energy (calculated via Poisson–Boltzmann method), and nonpolar solvation energy (estimated using solvent-accesible surface are, SASA). The average ΔG_bind and corresponding standard deviations were reported. Parameter choices (solute dielectric constant, number of snapshots, and omission of entropic terms) followed MM/PBSA benchmark studies on class A GPCRs and membrane proteins, particularly the systematic evaluation by Yau et al. (2019)[25] on twenty class A GPCR targets.

Markov state model construction

Markov state models (MSMs) were constructed using PyEMMA 2.5.7, following time-lagged independent component analysis (tICA) for dimensionality reduction. The MSMs were validated using data from three independent 1 μs replicate simulations per ligand to enhance ergodic sampling and ensure reproducibility of conformational states. Trajectories for each system were featurized based on the center-of-mass distances between transmembrane helices TM3 and TM6; χ_1 torsions key microswitch residues in the DRY (Arg165^3.50, Asp164^3.49) and NPxxY (Asn332^7.49, Tyr336^7.53) motifs; and Cα distances in intracellular loops (ICL2, ICL3).

tICA was performed with a lag time of 20 ns, retaining the top two independent components. The reduced space was discretized into 100 microstates via k-means clustering, and MSMs were constructed using the same lag time of 20 ns. Model quality was evaluated through convergence of implied timescales and Chapman–Kolmogorov tests to confirm metastable behavior. Macrostates were identified using PCCA++, typically resolving into 3–4 dominant basins. Transition kinetics were analyzed by computing mean first-passage times (MFPTs) between macrostates. Free energy surfaces (FES) were generated by projecting the trajectory data onto tIC1/tIC2 space and visualized as Boltzmann-weighted landscapes. All visualizations were rendered in matplotlib, using white backgrounds and antialiased vector graphics for publication-quality output.

Results and discussion

Molecular dynamics simulation revealed structural rearrangements induced by mitragynine binding

All-atom molecular dynamics simulations of 1 μs was conducted to investigate the impact of mitragynine binding on the μ-opioid receptor (μOR), in comparison to morphine - a well characterized, high-affinity synthetic μOR agonist. RMSD profiles across three replicates (Supplementary Fig. S1A–C) showed nearly identical convergence (mean ≈ 0.23 ± 0.03 nm), confirming reproducible equilibrium stability for both ligand systems.Morphine is a well characterized μOR agonist with high binding affinity and is known to stabilize the receptor in a fully active Gi-coupled conformation, as captured in the cryo-EM structure of μOR–morphine (PDB ID: 8EF6)[24]. In this study, the μOR was embedded in a fully hydrated POPC lipid bilayer during MD simulations to closely mimic the physiological membrane environment, allowing more realistic assessment of ligand-induced conformational dynamics (Fig. 1). This approach improved the biological relevance of the simulation results by incorporating membrane-protein interaction such as lipid-mediated allosteric effects, to correct the orientation and dynamics of transmembrane helices[26–28].

The root mean square deviation (RMSD) analysis (Fig. 2a) showed that the mitragynine-MOR complex stabilized at a slightly higher RMSD (~ 0.25 nm) with intermittent deviations, compared to the morphine-MOR complex, which exhibited stable RMSD values around ~ 0.20 nm. The root mean square fluctuation (RMSF) analysis (Fig. 2b) further revealed increased flexibility in the intracellular loop and transmembrane helix 6 (TM6) of the mitragynine-MOR complex, particularly between residues 261–315. These regions are known to undergo structural rearrangements during receptor activation and G protein engagement[29–31]. Morphine is a well-characterized full agonist of MOR, promoting a stable active conformation and strong G protein coupling[32–34]. In contrast, the increased flexibility observed in the intracellular loop and TM6 of the mitragynine-μOR complex suggested that mitragynine acts as a partial agonist, which may not fully stabilize the active conformation of μOR required for optimal G protein binding[1,35]. This interpretation was supported by the slightly higher RMSD of mitragynine-μOR complex, which indicated a higher flexibility of μOR to adopt broader range of conformations when bound to mitragynine compared to morphine. To further clarify how mitragynine engages the μOR binding pocket, we performed a detailed non-covalent interaction analysis across representative MD snapshots (100–1000 ns). As shown in Supplementary Fig. 2, mitragynine maintained a persistent hydrophobic network

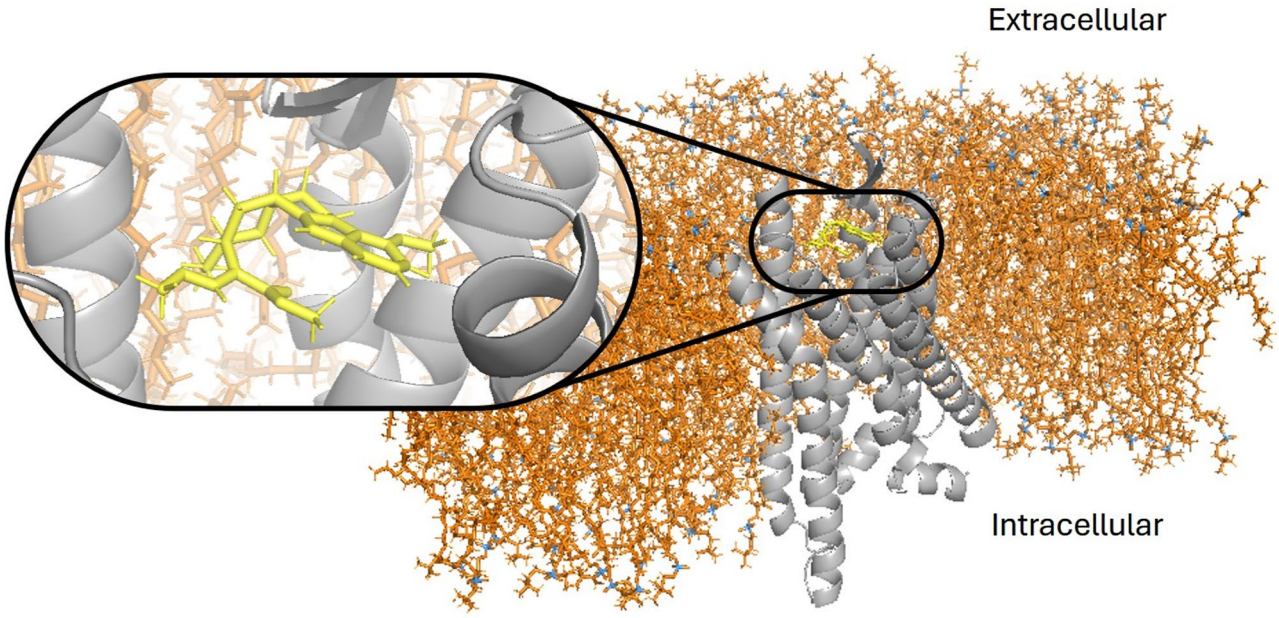

Fig. 1. Overall view of the μOR-mitragynine complex in a lipid bilayer. The μ-opioid receptor is shown embedded in lipid bilayer (orange sticks), and the μOR is displayed as a grey cartoon. The inset highlighted the binding site of mitragynine (yellow sticks) within the transmembrane domain.

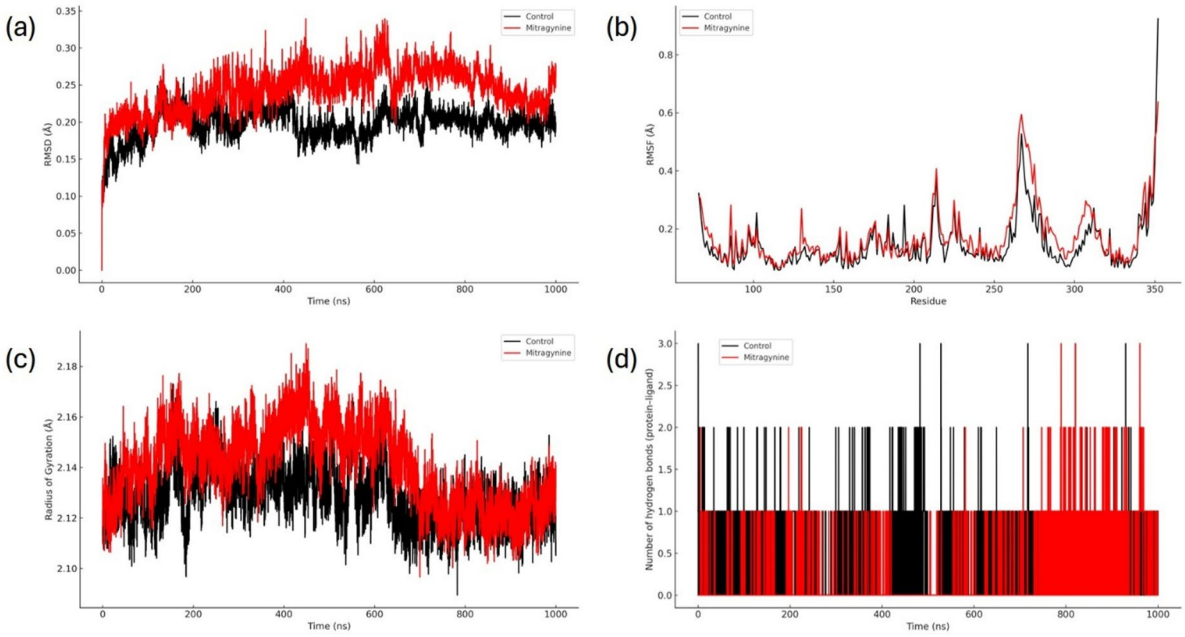

Fig. 2. Structural dynamics of μ-opioid receptor (MOR) complexes over 1000 ns molecular dynamics simulations. **a** Root mean square deviation (RMSD) of Cα atoms showed greater global conformational fluctuations in the mitragynine-bound μOR (red) compared to the morphine-bound μOR control (black); **b** Root mean square fluctuation (RMSF) showed increased flexibility of μOR upon mitragynine binding, particularly in intracellular loop and transmembrane helix 6 (TM6) (residue ~ 261–315); **c** Radius of gyration (Rg) analysis revealed increased structural fluctuations in the mitragynine-bound system during the 300–700 ns intervals, which stabilized after 800 ns to levels comparable with the control morphine-bound system; **d** Number of protein-ligand hydrogen bonds over 1000 ns simulation showed intermittent and less stable hydrogen bond interactions in the mitragynine-μOR complex relative to the control morphine-μOR complex.

with TRP135, ILE146, TYR150, LEU234, and TRP320, complemented by intermittent salt-bridge contacts with LYS235 and GLU231 and occasional hydrogen bonding with ASN232. This time-resolved analysis reveals that mitragynine stabilizes the receptor through a mixture of hydrophobic anchoring and transient polar interactions, consistent with its sampling of inactive and intermediate conformations. Notably, the mitragynine binding configuration observed in the present study differs from the binding mode previously reported by Zhou et al. (2020)[36], who employed an integrated computational framework comprising molecular docking, metadynamics-based rescoring, and four independent 250 ns molecular dynamics simulations, with additional validation through mutagenesis experiments. In their study, mitragynine was positioned within the canonical orthosteric pocket and stabilized through interactions involving conserved residues such as Asp147$^{3.32}$ and His297$^{6.52}$. In contrast, the present 1 μs all-atom simulations, performed in three independent replicates per ligand, revealed a dynamically stabilized binding configuration characterized predominantly by hydrophobic interactions with TRP135, ILE146, TYR150, LEU234, and TRP320, together with intermittent polar contacts. Supplementary Fig. 2 explicitly depicts these ligand–receptor interactions, including residue labeling and annotated interaction distances, allowing direct structural comparison between the two reported binding configurations. The observed differences likely reflect extended conformational relaxation captured during longer-timescale simulations in the present study.

The morphine-μOR complex also showed a consistent structural compactness (Fig. 2c), indicated a structurally stable μOR that aligned with full receptor activation upon morphine binding. But the radius of gyration (Rg) in mitragynine-μOR complex increased during 300–700 ns, suggested a transient expansion of the complex, possibly due to less stable conformational states. However, the Rg eventually stabilized and became comparable to that of the morphine-μOR complex, indicating a slower kinetic transition of the mitragynine-μOR complex toward a stable state. In addition, the mitragynine-μOR complex exhibited greater temporal variability in hydrogen bonding patterns (Fig. 2d), which appeared to be transient and dynamic compared to the more persistent hydrogen bonds observed in the morphine-μOR complex. Further assessment of the receptor-ligand conformational dynamics using principal component analysis (PCA) reinforced the hypothesis that mitragynine induces a more flexible conformational ensemble of μOR. The PCA plot revealed a tighter cluster for the morphine-μOR complex, which indicated a more restricted conformational space compared to a more dispersed cluster observed in the mitragynine-μOR complex, represented a broader conformational space due to higher structural flexibility (Fig. 3).

The combination of increased RMSD, elevated RMSF (residues ~ 261–315), transient increase in Rg, unstable hydrogen bonding in the mitragynine-μOR complex, and the PCA results collectively suggest that mitragynine binding induces a less rigid and more dynamic conformational ensemble of μOR[37]. These fluctuations are especially significant in cytoplasmic regions essential for μOR activation and G protein binding, indicating that mitragynine may induce μOR transitioning into intermediate or pre-active states, consistent with the proposed partial agonist behaviour compared to morphine as a full agonist[31,38]. Replicate-resolved PCA (Supplementary Fig. S3) showed that all three runs per ligand explore similar regions of PC1–PC2 space, confirming reproducibility. The mitragynine-bound μOR nonetheless samples a broader region than the morphine-bound control, consistent with a more heterogeneous, intermediate-rich conformational ensemble.

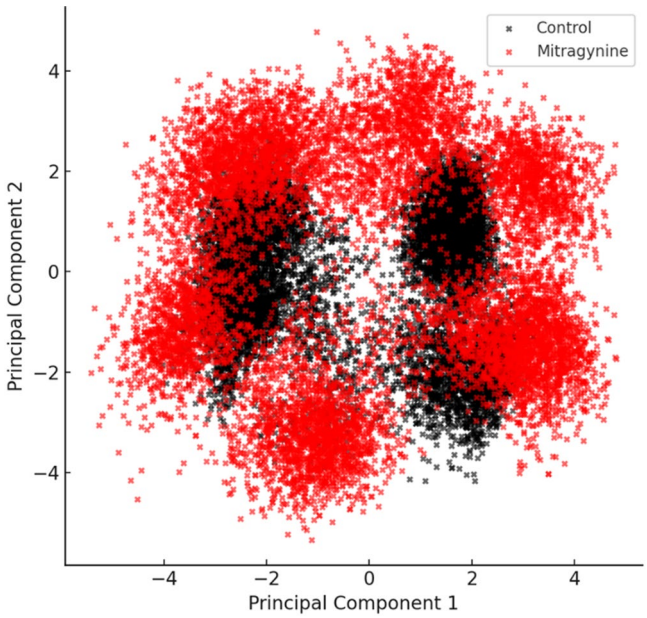

Fig. 3. Principal component analysis (PCA) of the μOR complexes bound to morphine (control - full agonist) and mitragynine. The scatter plot shows the projection onto principal component 1 and 2, which capture the major collective motions of the μOR in both complexes.

Energy component	morphine-μOR complex (control) kcal/mol	Mitragynine-μOR complex kcal/mol
VDWAALS	−26.89 ± 3.34	−35.57 ± 4.50
EEL	−13.77 ± 4.34	−7.09 ± 4.89
EPB	33.05 ± 5.33	30.48 ± 6.38
ENPOLAR	−3.17 ± 0.11	−4.13 ± 0.31
GGAS	−40.67 ± 5.09	−42.67 ± 5.93
GSOLV	29.88 ± 5.28	26.35 ± 6.27
Binding free energy, $\Delta G_{binding}$	−10.78 ± 4.22	−16.31 ± 5.12

Table 1. MMPBSA binding free energy and energy components of morphine- and mitragynine-MOR complexes. Data presented as means ± SD. *EEL* electrostatic interaction energy, *VDW* van der Waals interaction energy, *GGAS* gas-phase interaction energy (EEL + VDW), *EPB* polar solvation energy (Poisson–Boltzmann), *ENPOLAR* nonpolar solvation energy, *Gsolv* total solvation energy (EPB + ENPOLAR), *ΔGbind* estimated binding free energy.

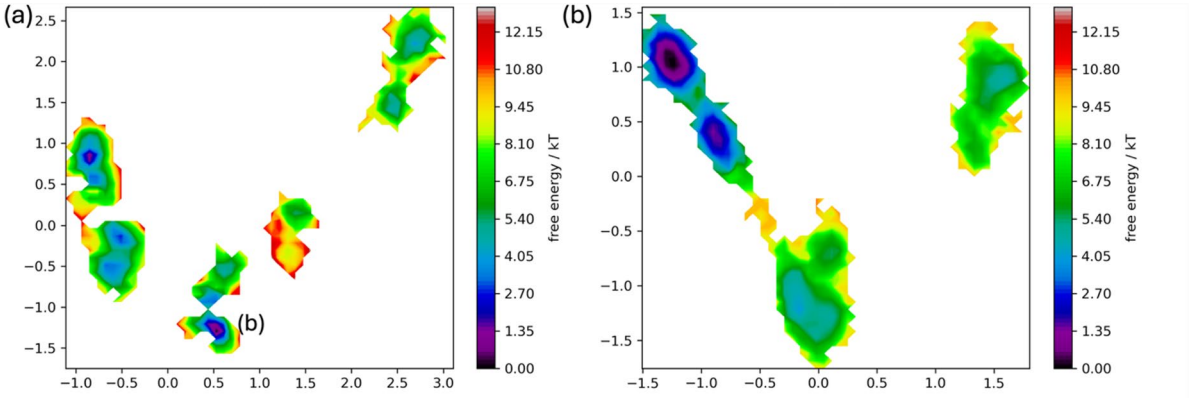

Fig. 4. Free-energy landscapes of μOR conformational states projected onto the first two time-lagged independent components (tIC1 and tIC2). **a** multiple compact basins in morphine-bound μOR separated by moderate barriers that scaled up to approximately 8 kT, showing several discrete metastable conformations, which include a deep basin that was consistent with an active-like state; **b** Elongated V-shaped valley with fewer but broader basins and higher energy barriers that scaled up to approximately 12 kT observed in mitragynine-bound μOR, suggested a free energy landscape that was dominated by intermediate-like conformations with reduced sampling of fully active conformations.

Mitragynine exhibits favorable binding energetics

The binding free energy ($\Delta G_{binding}$) calculations using MMPBSA revealed that both morphine (full agonist) and mitragynine (putative partial agonist) demonstrated favorable binding toward the μOR as indicated by negative $\Delta G_{binding}$ values (Table 1). Notably the mitragynine-μOR complex demonstrated a more favorable binding free energy (−16.31 ± 5.12 kcal/mol) compared to morphine-μOR complex (−10.78 ± 4.22 kcal/mol), suggesting a potentially stronger overall binding affinity of mitragynine toward MOR under the simulated conditions. However, decomposition of the energy components revealed distinct interaction profiles between morphine and mitragynine. A tighter hydrophobic interaction between mitragynine and MOR was deduced from the observed stronger van der Waals interactions (−35.57 ± 4.50 kcal/mol) compared to that of morphine (−26.89 ± 3.34 kcal/mol). Despite the stronger binding free energy predicted for mitragynine, it did not imply full receptor activation[21]. The previously described molecular dynamics analyses (RMSD, RMSF and PCA) suggested that mitragynine induced a more dynamic and flexible receptor conformation, especially in the regions critical for G protein coupling compared to the morphine that stabilized μOR in a more rigid and compact conformation characteristic of full activation.

MSM identifies distinct conformational landscapes

Markov state models (MSMs) revealed distinct differences in the conformational energy landscapes and kinetics of μOR upon binding of mitragynine compared to morphine. The free energy surfaces for morphine-μOR showed well-defined and deep basins, including a stable active-like state, whereas the mitragynine-μOR landscape was broader and dominated by intermediate conformations with shallow basins (Fig. 4).

This observation suggested that morphine shifted and strongly stabilized the fully active μOR conformation, while mitragynine-bound μOR stabilized in partially activated states. This aligned with general GPCR activation

theory where ligands of differing efficacy shifted the equilibrium of the receptor protein to multiple intermediate states[39]. Mitragynine exhibited partial agonism, allowing a larger population of intermediate states of μOR, effectively raising the barrier to reaching the fully open state. These observation matched experimental reports that mitragynine is a G-protein-biased partial agonist at μOR[1,4]. Subsequent implied timescales analysis from the MSMs further differentiated morphine-μOR and mitragynine-μOR systems (Fig. 5).

A well separated longest relaxation mode was observed in the morphine-μOR system (> 700 ns) (Fig. 5a), indicating a dominant slow transition between the closed and open basins. But timescales convergence of mitragynine-μOR system was below 400 ns (Fig. 5b), indicated rapid interchange among multiple states. Slower implied timescales corresponded to high free-energy barriers between metastable states, which was consistent with the deep active basin observed in morphine-μOR system (Fig. 4a). In GPCRs, the largest conformational changes, for instance, TM6 outward movement, involved overcoming substantial barriers and occurred on long timescales[39]. Slow mode observed in the morphine-μOR system likely represented the rare transition into or out of the active-like basin, which implied a stable active conformation. But shallow timescales observed in the mitragynine-μOR system suggested that the receptor rapidly sampled intermediates with lower barriers. This is in line with spectroscopic studies that have showed partial agonists populated new intermediate conformations rather than a single active state[39]. Thus, the markedly slower relaxation in the morphine-bound μOR provided kinetic evidence of a highly stabilized active state, whilst the faster timescales observed in mitragynine-μOR system implied facile interconversion among intermediate conformational ensembles.

Subsequent kinetic analysis revealed that the mean first-passage times (MFPTs) for transitions from intermediate (I) or closed (C) states to the open (O) state are much shorter for morphine-μOR system (hundreds of ns) (Fig. 6a) than for mitragynine-μOR system (microseconds) (Fig. 6b), indicated that the morphine-bound μOR can reach the active state faster. This indicated that morphine lowered the activation barrier for μOR effectively, consistent with its high efficacy. While mitragynine-bound μOR exhibited long MFPTs for I→O and C→O, implying that once μOR reached intermediate conformation it is kinetically stabilized. These differences in MFPTs aligned with classic pharmacology where full agonists rapidly induce activation, whereas partial agonists kinetically hindered activation. In mechanistic terms, morphine likely facilitated the rearrangements of the DRY, NPxxY, and toggle-switch motifs so that the receptor rapidly reaches the active conformation[39], but this pathway to full activation was retarded upon mitragynine binding, aligned to its partial agonist properties.

Consistently, the equilibrium macrostate populations was found to be significantly different. In the morphine-bound μOR MSM, the receptor populated both the closed (inactive) and open (active-like) macrostates. In contrast, the intermediate macrostate of μOR was significantly occupied in mitragynine-μOR system (Fig. 7a), with lower population in the closed and open states compared to morphine-μOR system. This dichotomy directly reflected ligand efficacy and signaling bias between morphine (full agonist) and mitragynine (partial agonist). Full agonists like morphine induced receptor conformational rearrangement into fully active ensemble to allow both G-protein and arrestin signalling, while mitragynine (partial agonist) stabilized an intermediate ensemble in the receptor. In fact, mitragynine is known experimentally to be G-protein-biased and not recruit β-arrestin[1]. The dominance of the intermediate state observed in MSM thus suggests that mitragynine-μOR adopted a conformation that engages G-proteins but does not adopt the fully open conformation required for arrestin binding. The differences in transition kinetics are further illustrated in Fig. 7b, where prolonged closed-to-open (c→o) and intermediate-to-open (i→o) transitions are evident in the mitragynine-bound system relative to morphine.

In addition to the MSM energy landscapes and kinetic analyses, structural snapshots of the three dominant macrostates were extracted for the mitragynine- and morphine-bound μOR (Fig. 8). To evaluate receptor

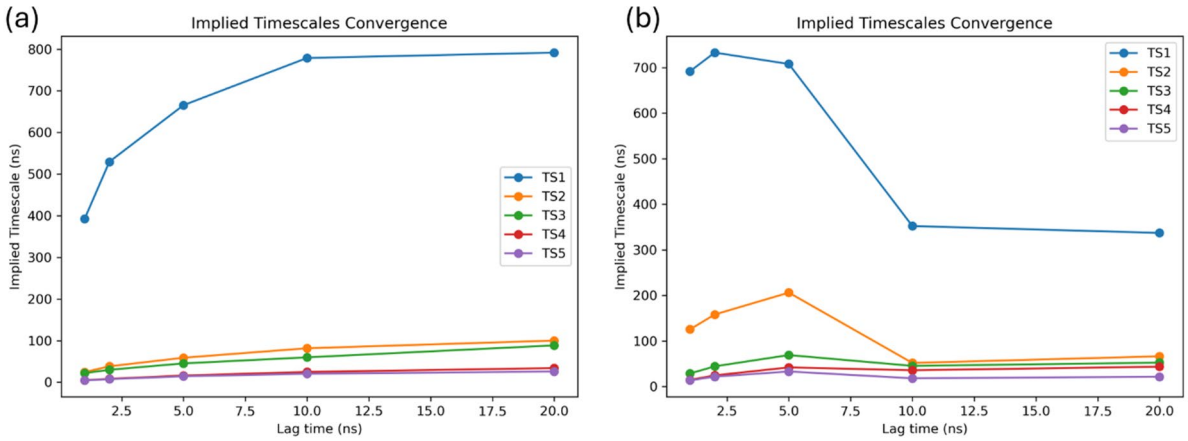

Fig. 5. Convergence of implied timescales as a function of lag time for Markov state model construction validation. **a** The morphine-bound μOR showed a dominant slow process that stabilized around 20 nanoseconds, consistent with a well-separated active-state transition; **b** The mitragynine-bound μOR showed a shorter slowest timescale with faster convergence, suggested a rapid interchange among intermediate states and weaker stabilization of a distinct active state compared to the control system (morphine-μOR).

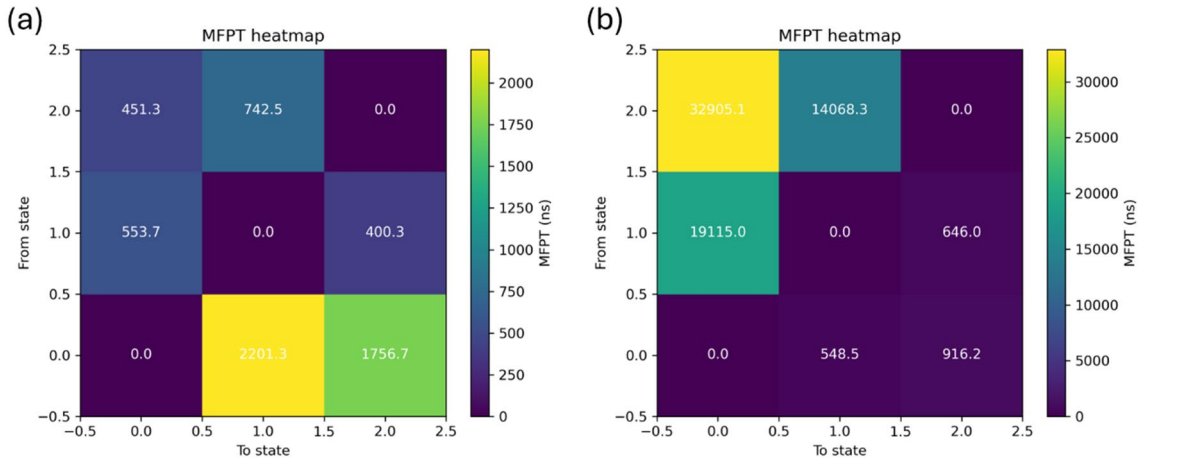

Fig. 6. Mean first-passage times heatmaps that illustrated the transition kinetics between different macrostates: closed, intermediate, and open. **a** Transitions between intermediate and open states of μOR upon morphine binding occurred within hundreds of nanoseconds with comparatively fast intermediate to open states and open to intermediate states, consistent with ready access to the active ensemble; **b** In the mitragynine-bound μOR, transitions particularly to the open state were markedly slower, with MFPTs extending into more than 10 microseconds, indicating kinetic hindrance that disfavoured direct progression to open state.

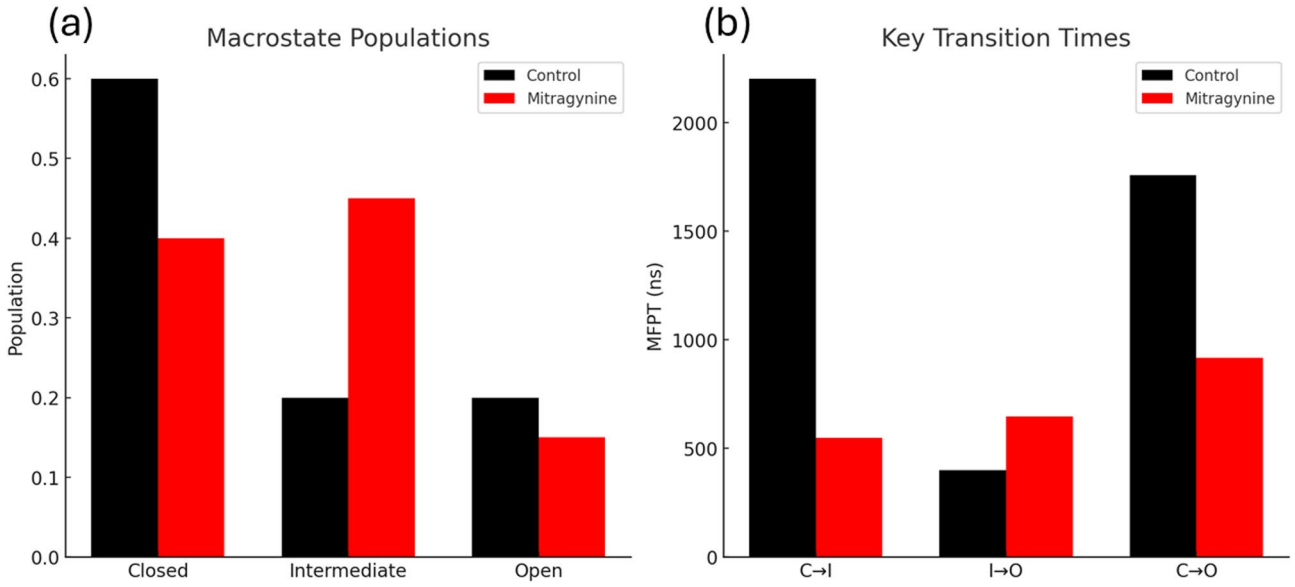

Fig. 7. Comparison of macrostate populations and key transition times between morphine- and mitragynine-bound μOR systems. **a** Morphine-bound μOR favoured closed to intermediate and open macrostates while mitragynine-bound μOR shifted weight toward intermediate macrostate, with lower open macrostate occupancy; **b** transition times reveal that morphine binding promoted faster progression from intermediate to open states (i→o), while mitragynine binding delayed the activation kinetics with prolonged closed to open (c→o) and intermediate to open (i→o) transitions, indicating a partial activation and stabilization of intermediate states.

activation, the canonical TM3–TM6 intracellular Cα–Cα distance between $Arg^{3.50}$ (chain A, residue 167) and $Leu^{6.34}$ (chain A, residue 277) was measured. This distance is a well-established indicator of GPCR activation, reflecting the outward movement of TM6 relative to TM3. In the mitragynine-bound μOR, the three dominant macrostates exhibited distances of 11.7 Å, 13.6 Å, and 14.6 Å, corresponding to inactive-to-intermediate conformations. In contrast, the morphine-bound control showed distances of 9.7 Å, 13.6 Å, and 14.5 Å, representing one deep-inactive and two intermediate-like states. These values are substantially shorter than the 16–20 Å spacing typically associated with the fully active receptor, indicating that both ligands predominantly stabilize intermediate ensembles during the microsecond-scale simulations. This observation supports the

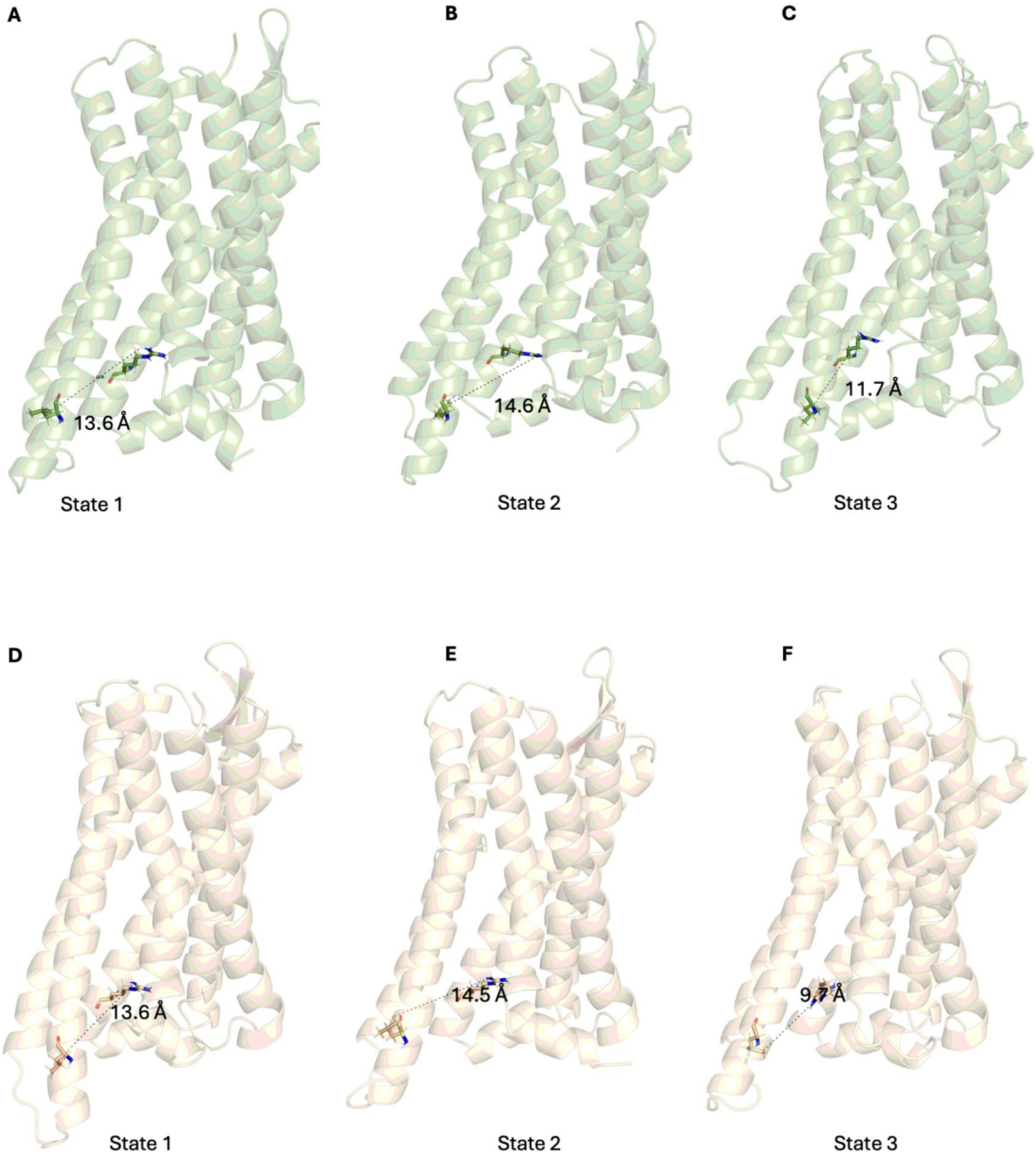

Fig. 8. Representative μOR macrostates showing the canonical TM3–TM6 activation metric. The intracellular activation distance was calculated between $Arg^{3.50}$ (chain A, residue 167) on TM3 and $Leu^{6.34}$ (chain A, residue 277) on TM6. **A–C** Mitragynine macrostates (11.7, 13.6, 14.6 Å) represent inactive-to-intermediate conformations. **D–F** Morphine macrostates (9.7, 13.6, 14.5 Å) correspond to deep-inactive and intermediate states. Interpretation bands: inactive ≈ 11–13 Å; intermediate ≈ 13–16 Å; active-like ≥ 16 Å. Both ligands sample inactive/intermediate separations rather than fully active spacing in the absence of G protein or nanobody.

notion that mitragynine behaves as a partial agonist, promoting limited TM6 displacement while lacking the full outward motion characteristic of the morphine-bound active receptor. To validate that our MSM macrostates correspond to biologically relevant μOR conformations, we compared the representative macrostates with high-resolution inactive and active μOR crystal structures (PDB ID: 4DKL and 8EF6). Supplementary Figure S4 shows that the mitragynine derived macrostates structurally overlap with the inactive 4DKL conformation, whereas the morphine-derived macrostates align more closely with the partially active 8EF6 structure. These overlays confirm that the MSM-derived intermediate states reproduce experimentally observed receptor geometries and that mitragynine primarily stabilizes inactive or intermediate ensembles while morphine extends sampling toward more active-like conformations.

In summary, the integrated MD and MSM analysis revealed that morphine and mitragynine possessed significantly different engagement with μ-opioid receptor. Morphine-bound μOR predominantly occupied a well-defined active-state basin, with rapid progression from intermediate states to open conformation. But mitragynine preferentially stabilized the μOR in intermediate conformations with slower activation kinetics

and overall greater structural flexibility. These conformational and kinetic differences observed in mitragynine-μOR system have aligned with experimentally observed mitragynine binding profile as G protein-biased partial agonist, promoted the receptor states that favour for G protein signalling while disfavouring β-arrestin engagement. This study highlighted the value of ensemble-based receptor modelling in comprehending ligand bias and the mitragynine scaffold as a potential starting point for designing μOR-targeted therapeutics with improved side-effect profiles.

Although each system was simulated for 1 μs across three replicates, it is important to acknowledge that GPCR activation and intermediate-state exchange occur on millisecond timescales[40–42]. Therefore, our trajectories primarily capture intermediate conformational sampling and ligand-dependent stabilization rather than full activation events, which remain consistent with the partial agonism mechanism explored in this study.

Data availability

The molecular dynamics trajectory files and Markov State Model datasets generated during the current study are not publicly available due to large file size, but are available from the corresponding author on reasonable request. All processed data supporting the findings of this study are included within this published article.

Received: 30 September 2025; Accepted: 3 March 2026
Published online: 07 March 2026

References

1. Kruegel, A. C. et al. Synthetic and receptor signaling explorations of the mitragyna alkaloids: mitragynine as an atypical molecular framework for opioid receptor modulators. *J. Am. Chem. Soc.* **138** (21), 6754–6764 (2016).
2. Inturrisi, C. E. Clinical pharmacology of opioids for pain. *Clin. J. Pain*. **18** (4), 3–13 (2002).
3. Pasternak, G. W. & Pan, Y. X. Mu opioids and their receptors: evolution of a concept. *Pharmacol. Rev.* **65** (4), 1257–1317 (2013).
4. Kruegel, A. C. & Grundmann, O. The medicinal chemistry and neuropharmacology of kratom: A preliminary discussion of a promising medicinal plant and analysis of its potential for abuse. *Neuropharmacology* **134**, 108–120 (2018).
5. Váradi, A. et al. Mitragynine/corynantheidine pseudoindoxyls as opioid analgesics with mu agonism and delta antagonism, which do not recruit β-arrestin-2. *J. Med. Chem.* **59** (18), 8381–8397 (2016).
6. Todd, D. A. et al. Chemical composition and biological effects of kratom (Mitragyna speciosa): In vitro studies with implications for efficacy and drug interactions. *Sci. Rep.* **10** (1), 19158 (2020).
7. Babu, K. M., McCurdy, C. R. & Boyer, E. W. Opioid receptors and legal highs: Salvia divinorum and Kratom. *Clin. Toxicol.* **46** (2), 146–152 (2008).
8. Zhao, Z., Huang, T. & Li, J. Molecular dynamics simulations to investigate how PZM21 affects the conformational state of the μ-opioid receptor upon activation. *Int. J. Mol. Sci.* **21** (13), 4699 (2020).
9. Zhou, Q. et al. Common activation mechanism of class A GPCRs. *eLife* **8**, e50279 (2019).
10. Shukla, D., Lawrenz, M. & Pande, V. S. Elucidating ligand-modulated conformational landscape of GPCRs using cloud-computing approaches. *Methods Enzymol.* **557**, 551–572 (2015).
11. Likhtenshtein, G. I. Molecular dynamics of proteins and their functional activity. In *Enzyme Catalysis Today and the Chemistry of the 21st Century* 247–278 (Springer, 2025).
12. Moradi, S. et al. A review on description dynamics and conformational changes of proteins using combination of principal component analysis and molecular dynamics simulation. *Comput. Biol. Med.* **183**, 109245 (2024).
13. Padhi, A. K., Janežič, M. & Zhang, K. Y. J. Molecular dynamics simulations: principles, methods, and applications in protein conformational dynamics. In *Advances in Protein Molecular and Structural Biology Methods* 439–454 (Elsevier, 2022).
14. Sokolov, M. & Cui, Q. Impact of fluctuations in the peridinin-chlorophyll a-protein on the energy transfer: Insights from classical and QM/MM molecular dynamics simulations. *Biochem* **64** (4), 879–894 (2025).
15. Aranda-Garcia, D. et al. Large scale investigation of GPCR molecular dynamics data uncovers allosteric sites and lateral gateways. *Nat. Commun.* **16**(1), 2020 (2025).
16. Li, M. et al. Delineating the stepwise millisecond allosteric activation mechanism of the class C GPCR dimer mGlu5. *Nat. Commun.* **15**(1), 7519 (2024).
17. Lopez-Balastegui, M. et al. Relevance of G protein-coupled receptor (GPCR) dynamics for receptor activation, signalling bias and allosteric modulation. *Br. J. Pharmacol.* **182**(14), 3211–3224 (2025).
18. Papasergi-Scott, M. M. et al. Time-resolved cryo-EM of G-protein activation by a GPCR. *Nature* **629** (8014), 1182–1191 (2024).
19. Duan, H., Zhao, D. R., Liu, M. T., Yang, L. Q. & Sang, P. Conformational remodeling and allosteric regulation underlying EGFR mutant-induced activation: A multi-scale analysis using MD, MSMS, and NRI. *Int. J. Mol. Sci.* **26**(13), 6226 (2025).
20. Ge, Y. & Voelz, V. A. Markov State Models to Elucidate Ligand Binding Mechanism. In *Protein-Ligand Interactions and Drug Design: Methods in Molecular Biology* Vol. 2266 (ed. Ballante, F.) 239–259 (Humana, 2021).
21. Dutta, S., Selvam, B. & Shukla, D. Mechanistic origin of partial agonism of δ9-tetrahydrocannabinol for cannabinoid receptors. *Biophys. J.* **120**(3), 131A-132A (2021).
22. Dutta, S., Selvam, B., Das, A. & Shukla, D. Mechanistic origin of partial agonism of tetrahydrocannabinol for cannabinoid receptors. *J. Biol. Chem.* **298**(4), 101764 (2022).
23. Bai, Q. et al. Conformation transition of intracellular part of glucagon receptor in complex with agonist glucagon by conventional and accelerated molecular dynamics simulations. *Front. Chem.* **7**, 851 (2019).
24. Zhuang, Y. et al. Molecular recognition of morphine and fentanyl by the human μ-opioid receptor. *Cell* **185** (23), 4361–4375 (2022).
25. Yau, M. Q., Liew, C. Y. & Ng, H. L. Evaluating the performance of MM/PBSA for binding affinity prediction using class A GPCR crystal structures. *J. Comput. Aided Mol. Des.* **33**, 487–503 (2019).
26. Jain, G. & Eddy, M. T. The influence of lipids and biological membranes on the conformational equilibria of GPCRs: Insights from NMR spectroscopy. *Curr. Opin. Struct. Biol.* **94**, 103103 (2025).
27. Jones, A. J. Y., Gabriel, F., Tandale, A. & Nietlispach, D. Structure and dynamics of GPCRs in lipid membranes: Physical principles and experimental approaches. *Molecules* **25** (20), 4729 (2020).
28. Stansfeld, P. J. et al. MemProtMD: Automated insertion of membrane protein structures into explicit lipid membranes. *Structure* **23**(7), 1350–1361 (2015).
29. Garcia-Nafria, J. & Tate, C. G. Cryo-EM structures of GPCRs coupled to Gs, Gi and Go. *Mol. Cell. Endocrinol.* **488**, 1–13 (2019).
30. Huang, W. et al. Structural insights into μ-opioid receptor activation. *Nature* **524** (7565), 315–321 (2015).
31. Kaneko, S. Activation mechanism of the μ-opioid receptor by an allosteric modulator. *Proc. Natl. Acad. Sci. USA.* **119**(16), e2121918119 (2022).
32. Munro, T. A. The μ opioid receptor crystal structure with BU72 is a covalent adduct. *ChemRxiv* (2022).

33. Munro, T. A. Reanalysis of a μ opioid receptor crystal structure reveals a covalent adduct with BU72. *BMC Biol.* **21**(1), 213 (2023).
34. Zádor, F., Király, K., Essmat, N. & Al-Khrasani, M. Recent molecular insights into agonist-specific binding to the mu-opioid receptor. *Front. Mol. Biosci.* **9**, 900547 (2022).
35. Alford, A. S., Moreno, H. L., Benjamin, M. M., Dickinson, C. F. & Hamann, M. T. Exploring the therapeutic potential of mitragynine and corynoxeine: Kratom-derived indole and oxindole alkaloids for pain management. *Pharmaceuticals* **18** (2), 222 (2025).
36. Zhou, L. et al. Molecular dynamics–based structural insights into the binding modes of mitragynine and its metabolites at the μ-opioid receptor. *Biochemistry* **59** (38), 3377–3390 (2020).
37. Chakraborty, S. & Majumdar, S. Natural products for the treatment of pain: Chemistry and pharmacology of salvinorin A, mitragynine, and collybolide. *Biochemistry* **60**(18), 1381–1400 (2020).
38. Kaneko, S. Structural and dynamic insights into the activation of the μ-opioid receptor by an allosteric modulator. *Nat. Commun.* **15**(1), 3544 (2024).
39. Weis, W. I. & Kobilka, B. K. The molecular basis of G protein-coupled receptor activation. *Annu. Rev. Biochem.* **87** (1), 897–919 (2018).
40. Latorraca, N. R., Venkatakrishnan, A. J. & Dror, R. O. GPCR dynamics: Structures in motion. *Chem. Rev.* **117**(1), 139–155 (2017).
41. Dror, R. O. et al. Activation mechanism of the β2-adrenergic receptor. *Proc. Natl. Acad. Sci. U.S.A.* **108**(46), 18684–18689 (2011).
42. Zhang, M. et al. G protein-coupled receptors (GPCRs): Advances in structures, mechanisms and drug discovery. *Signal Transduct. Target. Ther.* **9**(1), 88 (2024).

Acknowledgements

The authors would like to thank all colleagues and institutions that supported this research.

Author contributions

M.A.M.J. conceived and designed the study, performed molecular dynamics simulations and Markov State Modelling analyses, and wrote the main manuscript text. L.C.F. carried out computational analyses, prepared figures, and contributed substantially to manuscript preparation. M.N.A.B. performed molecular dynamics simulations and assisted in data analysis. L.A. contributed to methodology, validation, and manuscript editing. A.S. provided supervision, resources, and critical revision of the manuscript. E.K.P. supervised the project, secured funding, and contributed to conceptualization and final revision. A.A.M. assisted with project administration and data interpretation. All authors reviewed and approved the final manuscript.

Funding

This research was funded by the Ministry of Higher Education, Malaysia, under the Fundamental Research Grant Scheme Early Career with reference code: FRGS-EC/1/2024/STG01/USIM/03/3).

Declarations

Competing interests

The authors declare no competing interests.

Additional information

Supplementary Information The online version contains supplementary material available at https://doi.org/10.1038/s41598-026-43251-y.

Correspondence and requests for materials should be addressed to M.A.M.J.